pp 212–229. © Royal Aeronautical Society 2019
doi:10.1017/aer.2018.151

Peripheral milling-induced residual stress and its effect on tensile–tensile fatigue life of aeronautic titanium alloy Ti–6Al–4V

Dong Yang
yangdong@ahu.edu.cn
Department of Mechanical Engineering
Anhui University
Hefei
China

Xiao Xiao
Hefei Science and Technology College
Hefei
China

Yulei Liu
Department of Mechanical Engineering
Anhui University
Hefei
China

Jing Sun
Hefei Science and Technology College
Hefei
China

ABSTRACT

The special application environment puts forward the higher requirement of reliability of parts made from titanium alloy Ti–6Al–4V, which is closely related to the machining-induced residual stress. For the fact of the non-linear distribution of residual stress beneath the machined surface, distribution of peripheral milling-induced residual stress and its effect on

Received 7 May 2018; revised 15 October 2018; accepted 18 October 2018.

fatigue performance of titanium alloy Ti–6Al–4V are still confusing. In the present study, residual stress profile induced by peripheral milling of Ti–6Al–4V is first studied. And then, energy criteria are proposed to characterise the whole state of the residual stress field. Finally, the effects of residual stress profile and surface energy on tensile–tensile fatigue performance of titanium alloy Ti–6Al–4V are discussed. The conclusions were drawn that the variation trend of surface residual stress ($\sigma_{r,Sur}$), maximum compressive residual stress ($\sigma_{C,ax}$), location (h_{r0}) and response depth (h_{ry}) of residual stress profile with cutting parameters showed a similar pattern for both measure directions those parallel (σ_1) and perpendicular (σ_3) to the cutting direction. Cutting speed and feed rate have a main effect on surface residual stress, and the depth of cut has little effect on all the four key factors of residual stress profile. With the increase of cutting speed and feed rate, machining-induced surface energy tends to become larger. But increasing the depth of cut caused the strain energy stored in unit time to decrease. Furthermore, the effect of depth of cut on surface energy was weakened when the value of cutting depth becomes larger. Both the surface compressive residual stress and the maximum compressive residual stress are beneficial for prolonging the fatigue life, while large value of machining-induced surface energy leads to a decrease of fatigue life. Analysis of variance result shows that maximum residual compressive stress has a greater impact on fatigue life than other residual stress factors.

Keywords: Peripheral milling; Residual stress; Surface energy; Fatigue life; Titanium alloy Ti–6Al–4V

NOMENCLATURE

$\sigma_{r,Sur}$	surface residual stress (MPa)
$\sigma_{C,ax}$	maximum compressive residual stress (MPa)
h_{r0}	depth to the machined surface of $\sigma_{C,ax}$ (μm)
h_{ry}	response depth of residual stress (μm)
P_ε	strain energy density (J/m^2)
P_d	distortional strain energy density (J/m^2)
P_v	dilatational strain energy density (J/m^2)
σ_1, σ_2 and σ_3	three principal stresses in three-dimensional space (MPa)
ε_1, ε_2 and ε_3	strains in the directions of three principal stresses
E	Young's modulus of titanium alloy Ti–6Al–4V (GPa)
μ	Poisson ratio of titanium alloy Ti–6Al–4V
C_o	amplitude constant (MPa)
φ	phase angle (In degree)
ς	damping coefficient
w_d	damped frequencies (μm^{-1})
v_f	feed speed (m/s)
a_e	width of cut (mm)
Z	number of teeth
v_c	cutting speed (m/min)
f_z	feed per tooth (mm)
σ_s	yield limit of titanium alloy Ti–6Al–4V (MPa)
σ_a	stress amplitude (MPa)
R_0	stress ratio

https://doi.org/10.1017/aer.2018.151 Published online by Cambridge University Press

1.0 INTRODUCTION

Titanium alloy Ti–6Al–4V is widely used in the aviation, aerospace, enginery and other manufacturing industries for its excellent combination of properties, such as high strength to weight ratio, good fracture toughness and strong resistance to corrosion[1]. In these applications, the components are always subjected to cyclical mechanical and thermal loads, and thus, it puts forward higher requirement of reliability of parts, which is directly related to surface integrity of the product achieved by final machining.

For the past several decades, many researches have been carried out on machining-induced surface integrity and its effect on fatigue performance. In most of these studies, fatigue life is generally regarded as the function of surface integrity indictors, such as surface topography and residual stress and micro-hardness. Zhang et al. found that the logarithm of surface roughness or surface micro-crack presents the relationship of a quadratic curve with fatigue life, and fatigue life decreases with an increase of surface roughness[2]. Javidi et al. found that an increase of compressive residual stress causes an increase of fatigue life through the study of the effect of surface integrity on fatigue life of 34CrNiMo6[3]. Meanwhile, the effect of residual stress on fatigue life is found to have more pronounced than the effect of surface roughness. Due to the presence of highly compressive surface residual stresses caused by the turning operation, explained by Sharman et al. that the turned specimens to have a higher fatigue strength than electro-chemical machined and electro-discharge textured specimens made from Ti–45Al–2Nb–2Mn + 0.8 vol% TiB2 alloy[4]. Liu et al. concluded that the softened layer below the work-hardened surface and the compressive residual stress field were regarded as the two main reasons to prolong the fatigue life of the machined surface, which was drawn on the basis of face milling and three points bending fatigue life tests of 17-4PH stainless steel[5]. Li et al. found that the fatigue limit of Ti–6Al–4V can be improved with the increase of surface compressive stress under a given stress ratio, while this effect drops with an increase of stress ratio. The region where crack initiates is also affected by the distribution status of residual compressive stress on the material surface[6].

According to the conclusions of previous studies, the fatigue performance of the machined workpiece is determined by the interactions of the above-mentioned surface integrity indictors, but one generally accepted way to improve fatigue resistance is to induce a compressive residual stress in the surface layers of the material, making the nucleation and propagation of fatigue cracks more difficult. However, the influence of machining-induced residual stress distribution on fatigue performance is still confusing. Smith et al. found that the fatigue life is directly proportional to both the surface compressive residual stress and the maximum compressive residual stress in their study on the relationship between surface integrity and fatigue life of hard turned AISI 52100 steel[7]. Farrahi et al. worked with the AFNOR 60SC7 spring steel and showed that fatigue life improvement is owing to the maximum residual stress and also the depth of the response depth of residual stress. A correlation was found between the fatigue life and the area-under-the-residual stress curve[8]. Guo et al. found that the slope of the compressive residual stress profile was an important factor in rolling contact fatigue damage, and they also demonstrated that the relative fatigue damage can be characterised by multi-axial fatigue damage parameters under the influence of machining-induced residual stress profiles[9,10]

In aspect of cutting parameters on machining-induced residual stress, Sun claims for milling Ti–6Al–4V that an increase in feed rate makes the residual stresses more tensile at the surface, and with increasing cutting speed, surface residual stresses becomes more

https://doi.org/10.1017/aer.2018.151 Published online by Cambridge University Press

compressive[11]. Sridhar confirmed that the form of surface stress got more compressive with the increase of cutting speed when milling IMI-834[12]. However, Guerville claimed the opposite to Sridhar's conclusion, and that is more tensile residual stresses are generated with increasing cutting speed[13]. Mantle also found that compressive stresses decreased when the cutting speed was increased in milling gamma-titanium aluminide[14]. Thus, it is difficult to achieve a unified conclusion on the influence of cutting parameters on the machining-induced residual stresses. Furthermore, residual stress distribution characteristics in peripheral milling of titanium alloy Ti–6Al–4V have received little coverage in the previous literatures.

Following the analysis given above, there are two problems needing to be solved. On the one hand, sensitivity of cutting parameters of peripheral milling-induced residual stress profile and its overall state are not well identified. On the other hand, the correlation between the machining-induced residual stress and fatigue performance needs to be revealed. In the present study, residual stress profile induced by peripheral milling of Ti–6Al–4V is first studied. And then an energy criterion for machining-induced residual stress field, named surface energy, is proposed to characterise the whole stated of the residual stress field. Finally, the effects of residual stress profile and surface energy induced by peripheral milling on tensile–tensile fatigue performance of titanium alloy Ti–6Al–4V are discussed.

2.0 CHARACTERISATION OF MACHINING-INDUCED RESIDUAL STRESS

In this section, profile and the overall state of machining-induced residual stress are characterised.

2.1 Residual stress profile induced by machining

Under the action of cutting load, the newly formed surface undergoes forced compression to cause plastic deformation, and as the force is removed the material undergoes partial, but not a full recovery, due to the permanent deformation that has occurred. The material further from the machined surface which is only elastically deformed, springs back from the compression state and forces the plastically deformed material closer to the machined surface into tensile (or small compressive). Therefore, as shown in Fig. 1, four key factors of the residual stress profile can be identified as surface residual stress ($\sigma_{r,Sur}$), maximum compressive residual stress ($\sigma_{C,ax}$) and location (h_{r0}), response depth (h_{ry})[15].

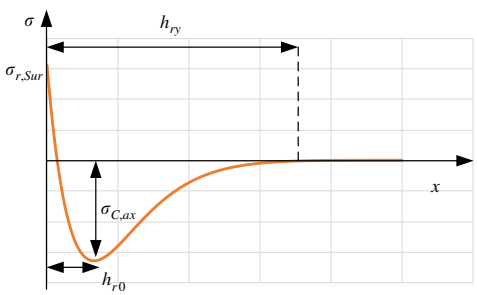

Figure 1. (Colour online) Residual stress profile induced by machining.

https://doi.org/10.1017/aer.2018.151 Published online by Cambridge University Press

2.2 Energy criteria for residual stress field

Machining-induced residual stress field is actually the energy field that stores strain energy input by cutting system and dissipated by various forms, such as plastic deformation and fracture.

The residual stress field after cutting is in the state of self-balance, therefore, the plastic deformation history during the machining process is not been considered in the present study. In addition, the assumption is also made that the studied material is an isotropic material. On the basis of the elastic-plasticity theory, the strain energy density P_ε of one certain point in the residual stress field can be expressed as follows:

$$P_\varepsilon = \frac{1}{2}\sigma_1\varepsilon_1 + \frac{1}{2}\sigma_2\varepsilon_2 + \frac{1}{2}\sigma_3\varepsilon_3 \quad \ldots(1)$$

where σ_1, σ_2 and σ_3 are the three principal stresses in three-dimensional space; ε_1, ε_2 and ε_3 are the strains in the directions of three principal stresses, respectively.

The strain energy density P_ε is the sum of distortional strain energy density P_d and dilatational strain energy density P_v, where P_v can be expressed as follows:

$$P_v = \frac{3}{2}\sigma_m\varepsilon_m = \frac{1-2\mu}{6E}(\sigma_1+\sigma_2+\sigma_3)^2 \quad \ldots(2)$$

where σ_m, ε_m are the mean values of principal stresses and principal strains. E and μ are the Young's modulus and the Poisson ratio of the material, respectively.

As a consequence, the distortional strain energy density v_d can be expressed as follows:

$$P_d = P_\varepsilon - P_v = \frac{1+\mu}{6E}\left[(\sigma_1-\sigma_2)^2 + (\sigma_2-\sigma_3)^2 + (\sigma_1-\sigma_3)^2\right] \quad \ldots(3)$$

Considering that the machining-induced residual stress is usually distributed only in the shallow part of the workpiece, the normal stress σ_2 in the direction perpendicular to the machined surface is approximately zero. Meanwhile, it is assumed that the volume does not change during the plastic deformation process, and the value of μ is 0.5. Therefore, the equation of strain energy density is updated as follows:

$$P_\varepsilon = P_d = \frac{1}{2E}(\sigma_1^2 + \sigma_3^2 - \sigma_1\sigma_3) \quad \ldots(4)$$

The machining-induced residual stress is a function of the depth from the machined surface, and it is the same for the strain energy density. For the purpose of describing the strain energy density by a general function, an exponential cosine attenuation function, which is described as Equation (5), is proposed. It is proved in the author's previous work that the exponential cosine attenuation function has a high precision to represent the hook distribution feature of the machining-induced residual stress profile[15]:

$$\sigma(x) = C_0 e^{-\frac{\zeta w_d x}{\sqrt{1-\zeta^2}}}\cos(w_d x + \varphi) \quad \ldots(5)$$

where $\sigma(x)$ is the value of residual stress at a given depth x to the machined surface. C_0 is the amplitude constant, φ is the phase angle and these two parameters determine the value of residual stress at any position below the machined surface. ς is the damping coefficient, which indicates the attenuation of the residual stress profile. w_d is the damped frequencies, which is related to the periods of the residual stress profile.

https://doi.org/10.1017/aer.2018.151 Published online by Cambridge University Press

Combined Equations (4) and (5), the strain energy density P_ε is updated as follows:

$$P_\varepsilon = \frac{1}{2E}\left[\sigma_1^2(x) + \sigma_3^2(x) - \sigma_1(x)\sigma_3(x)\right] \quad \ldots(6)$$

Therefore, the strain energy stored in unit time during the machining process can be drawn as follows:

$$P_{\text{cut}} = \frac{v_f a_e}{2E}\int_0^{h_{ry}} \left[\sigma_1^2(x) + \sigma_3^2(x) - \sigma_1(x)\sigma_3(x)\right] \mathrm{d}x \quad \ldots(7)$$

where v_f , a_e are the feed speed and width of cut, respectively. And the feed speed v_f can be calculated by the following equation:

$$v_f = \frac{v_c f_z Z}{60\pi d}(\text{m/s}) \quad \ldots(8)$$

where Z is the number of teeth in milling cutter.

On the basis of the assumption that the distribution of residual stresses is uniform beneath the machined surface, the strain energy stored into the workpiece material in unit time during the machining process can be used to characterise the overall state of machining-induced residual stress.

3.0 MATERIAL AND EXPERIMENTS

3.1 Material and cutting experiments

The material studied was two phase titanium alloy Ti–6Al–4V. As shown in Fig. 2, two kinds of phases named α and β are included, where the α phase is shown in black while the β phase is white. The chemical compositions of Ti–6Al–4V are as follows (wt%): 4.83–6.8% Al, 3.5–4.5% V, < 0.25% Fe, < 0.05% N , < 0.2 O and balance Ti.

Figure 3 shows a schematic diagram of the sample used. Different processing techniques were applied for surface A and surface B to exclude the effect on fatigue performance, surface A is processed by end milling, grinding and polishing with the same machining parameters for all the specimen. While for surface B, the investigated surface, peripheral milling (as shown in Fig. 4) was conducted under different cutting parameters. A three factor and four level orthogonal experiment was designed to get different residual stress fields of surface B, and the cutting speed v_c, feed per tooth f_z and radial depth of cut a_e are given in Table 1.

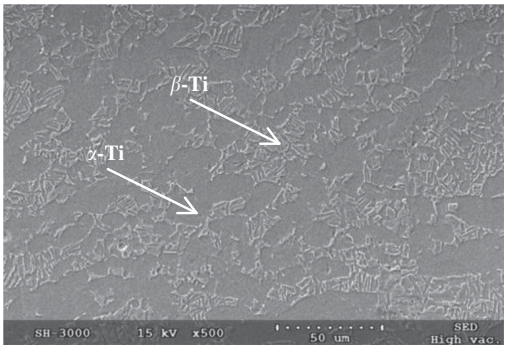

Figure 2. Microstructure of Ti–6Al–4V alloy.

https://doi.org/10.1017/aer.2018.151 Published online by Cambridge University Press

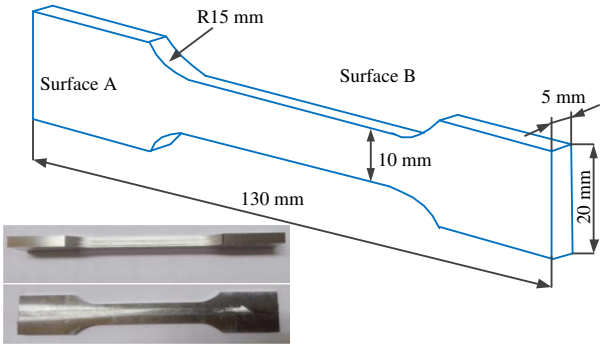

Figure 3. (Colour online) Fatigue specimen.

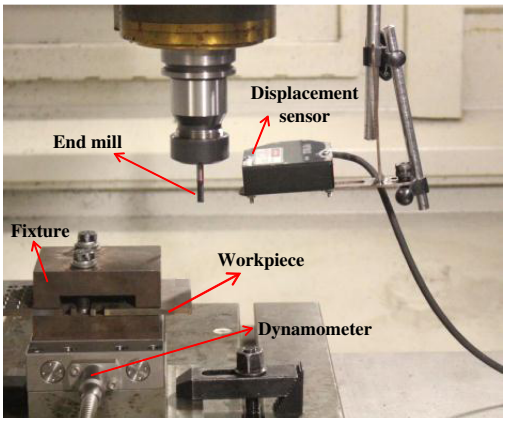

Figure 4. (Colour online) Set-up of the peripheral milling test.

Table 1
Cutting process parameters

	Cutting parameters				Cutting parameters		
	v_c	f_z	a_e		v_c	f_z	a_e
No.	**m/min**	**mm/z**	**mm**	**No.**	**m/min**	**mm/z**	**mm**
G01	20	0.02	1.0	G09	80	0.02	2.0
G02	20	0.03	1.5	G10	80	0.03	0.5
G03	20	0.04	2.0	G11	80	0.04	1.0
G04	20	0.05	0.5	G12	80	0.05	1.5
G05	50	0.02	1.5	G13	110	0.02	0.5
G06	50	0.03	1.0	G14	110	0.03	2.0
G07	50	0.04	0.5	G15	110	0.04	1.5
G08	50	0.05	2.0	G16	110	0.05	1.0

https://doi.org/10.1017/aer.2018.151 Published online by Cambridge University Press

Table 2
Parameters of the electro-chemically polished method[16]

Chemical compositions	$HClO_4$	30 ml
	N-Butyl alcohol	175 ml
	Methanol	300 ml
Electrolytic parameters	Voltage	17 V
	Current density	0.05–0.10 A/cm^2
	Polishing rate	25 nm/s
Environment	Room temperature (25°C)	

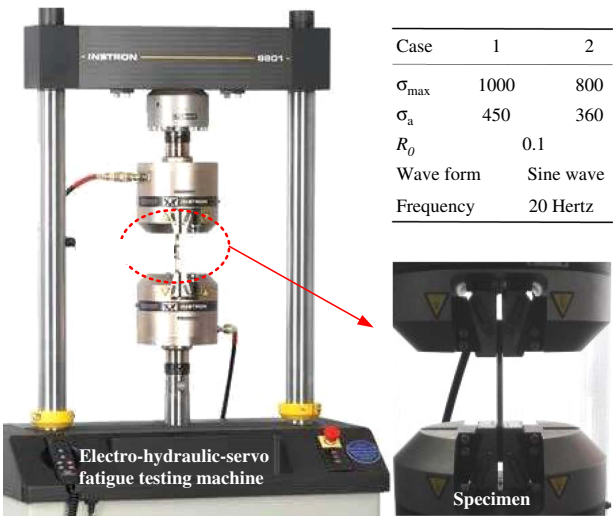

Case	1	2
σ_{max}	1000	800
σ_a	450	360
R_0	0.1	
Wave form	Sine wave	
Frequency	20 Hertz	

Figure 5. (Colour online) Fatigue experiments equipment and experimental conditions.

The machining experiments were carried out on a vertical type machining center (DAE-WOOACE-V500). The diameter of the cutter was 6 mm with 4-flute tool with variable helix angles (38° and 41°), which is made from cemented carbide. The experiments were performed with dry machining and the milling mode was down milling.

3.2 Residual stress measured

A Proto-LXRD diffractometer with Cu Kα radiation tube was used to measure the residual stresses of Ti–6Al–4V induced by peripheral milling. The collimator diameter is 1mm. Tube voltage and current are 30 kV and 25 mA, respectively. The (213) crystallographic planes of α phase of titanium alloy Ti–6Al–4V were measured, and the peak position 2θ is 139.47°. Nickel filters were applied to reduce the intensity of copper K-β radiation. Two position sensitive scintillation detectors were used to cover all ranges of ψ angles. Residual stresses of all test positions were measured in two directions: parallel (σ_1) and perpendicular (σ_3) to the cutting direction in the machined surface, and all these parameters were taken at three locations and repeated twice at each location.

https://doi.org/10.1017/aer.2018.151 Published online by Cambridge University Press

In addition, the electro-chemically polished method was applied to get the residual stress profile in machined surface layer, and the test positions are 2 μm, 4 μm, 6 μm, 8 μm, 10 μm, 20 μm, 40 μm, 60 μm and 80 μm beneath the machined surface. Parameters of the electro-chemically polished method are listed in Table 2.

3.3 Fatigue tests

As shown in Fig. 5, the tensile–tensile fatigue experiments were carried out on the Instron 8801 electro-hydraulic-servo fatigue testing machine at room temperature. Stress control was adopted in the form of a sine wave with a frequency of 20 Hz. Two kinds of loading conditions were applied. In case 1, maximum fatigue alternating stress σ_{max} is 1,000 MPa, which is larger than the yield limit σ_s (894–903 MPa) of the studied material. Stress amplitude σ_a and stress ratio R_0 are 450 MPa and 0.1. And in case 2, the maximum fatigue alternating stress σ_{max} is 800 MPa, which is smaller than the yield limit σ_s of the studied material. Stress amplitude σ_a and stress ratio R_0 are 360 MPa and 0.1, respectively. In the present study, the fatigue experiments under the same cutting conditions are repeated three times, and the average value is used to characterise the fatigue performances of the specimens.

4.0 RESULTS AND DISCUSSION

In this section, peripheral milling-induced residual stress profile and its energy index were first characterised, and the sensitivity of them to the cutting parameters was analysed. Second, the influences of residual stress profile and surface energy on fatigue life were discussed.

4.1 Machining-induced residual stress profile

As shown in Fig. 6, the residual stress profile of titanium alloy Ti–6Al–4V induced by peripheral milling follows a similar pattern, a compressive (or small tensile) peak at the machined surface, followed by a compressive peak, settling at a distance without positive again, or very small positive values. It also can be found that the value of the maximum compressive stress can reach 600 MPa in the place of approximately 2–10 μm beneath the machined surface, and the response depth of residual stress is less than 100 μm.

On the basis of the measured residual stress profile, four key factors $\sigma_{r,Sur}$, $\sigma_{C,ax}$, h_{r0} and h_{ry} were identified, and their sensitivity to cutting parameters were drawn as follows.

Values of the four key factors $\sigma_{r,Sur}$, $\sigma_{C,ax}$, h_{r0} and h_{ry} of the measured residual stress profile, and their relationship with cutting parameters are summarised in Fig. 7. It can be seen that the four factors of σ_1 and σ_3 show a similar variation trend, both values of $\sigma_{r,Sur}$ and $\sigma_{C,ax}$ of σ_1 are larger than those of σ_3, while h_{r0} and h_{ry} of σ_1 are smaller than those of σ_3. Compared to v_c and f_z, a_e has little effect on the four key factors of residual stress profile. In addition, the changes of h_{r0} and h_{ry} with the cutting parameters are not obvious, and this is mainly due to two reasons, first, thermo-mechanical coupling effect induced by peripheral milling under the presented cutting conditions has a small change. Second, values of h_{r0} and h_{ry} are small, and limited spacing test points are selected considering the accuracy of XRD method. In aspects of $\sigma_{r,Sur}$ and $\sigma_{C,ax}$, both $\sigma_{r,Sur}$ values of σ_1 and σ_3 decreased with the increase of cutting speed. While increase trends are found for $\sigma_{C,ax}$ by increasing the cutting speed, and it is more significant for σ_3. When f_z was changed from 0.02 mm to 0.05 mm, the values of $\sigma_{r,Sur}$ and $\sigma_{C,ax}$ of σ_1 decreased significantly, and the variations of $\sigma_{r,Sur}$ and $\sigma_{C,ax}$ of σ_1 against f_z were pretty minute.

https://doi.org/10.1017/aer.2018.151 Published online by Cambridge University Press

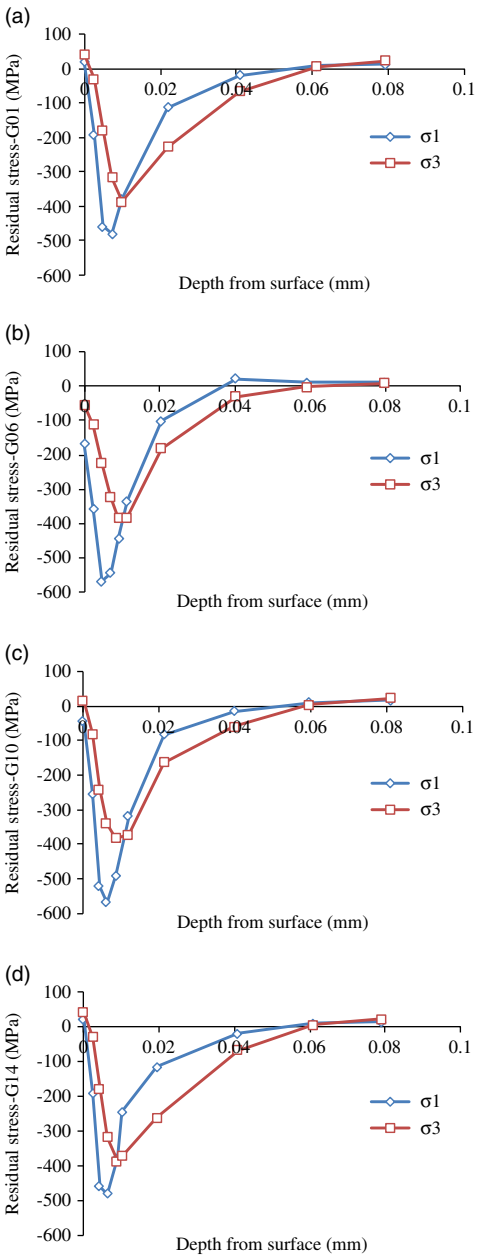

Figure 6. (Colour online) In-depth distribution of machining-induced residual stress.

4.2 Machining-induced surface energy

To get the machining-induced surface energy parameter P_{cut}, four coefficients in Equation (5) were optimised subsequently. A multi-objective optimisation method is needed to fulfill the work, and particle swarm optimisation (PSO) method is applied in the present study. PSO is an evolutionary method similar to genetic algorithms, which is widely used for machining

https://doi.org/10.1017/aer.2018.151 Published online by Cambridge University Press

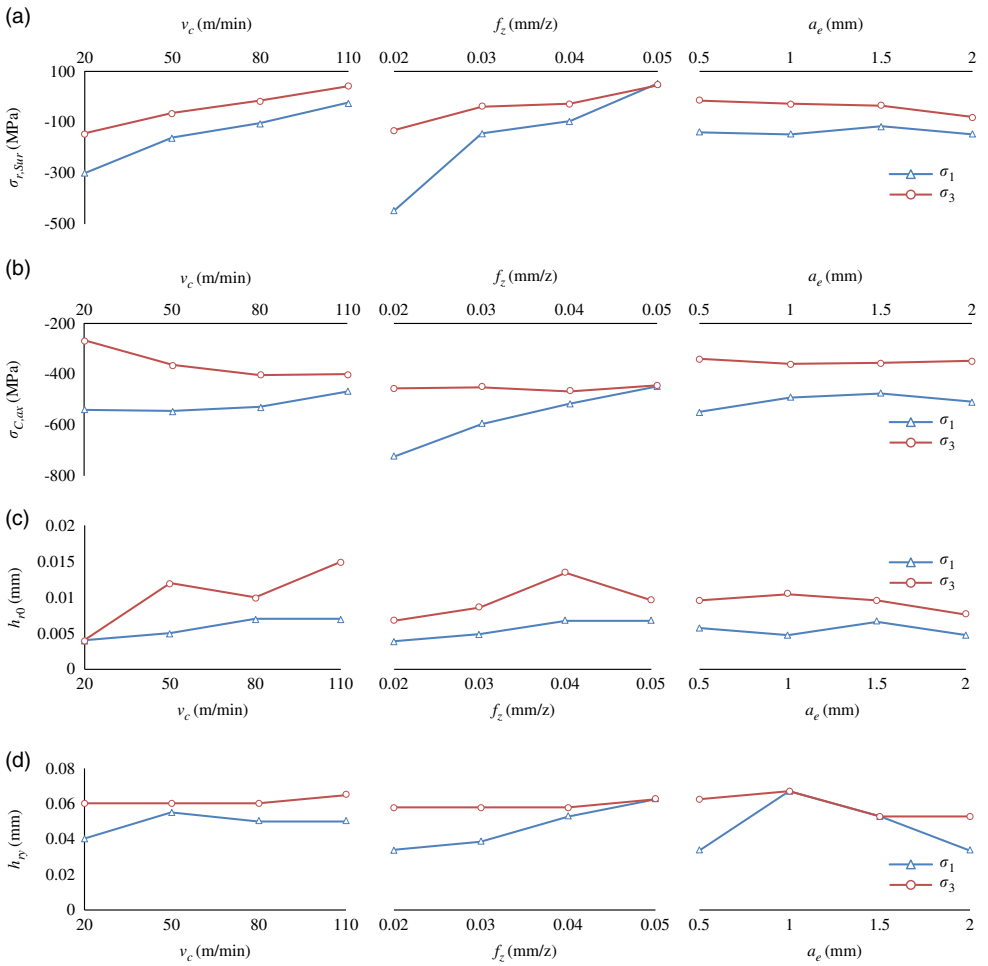

Figure 7. (Colour online) Relationship of (a) $\sigma_{r,Sur}$, (b) $\sigma_{C,ax}$, (c) h_{r0} and (d) h_{ry} with cutting parameters.

process optimisation[17]. In PSO algorithm, the population has n_p particles that represent candidate solutions. Each particle is a m_p dimensional real valued vector where m_p is the number of optimised parameters, and each optimised parameter represents a dimension of the problem space. The flow chart of PSO method is shown in Fig. 8.

The surface stress is represented with both phase angle and amplitude, so there is no need to have restrictions on the values of φ and C_0 in Equation (5). In the present study, the amplitude is ranged from 0 to 1,000 MPa, and phase angle is set in the range of $[-\pi, +\pi]$. The damped frequency is proportional to the inverse of the period of the wave, and since it was estimated that the function would settle less than 100 μm, ω_d is in the range [0, 200] μm^{-1}. Since the desired shape is under damped, the damping coefficient (ς) is mathematically upper-limited at 1. On the other hand, if a wave is only slightly damped (e.g. $\varsigma < 0.5$), it would oscillate between positive and negative many times, and the residual stress profiles conventionally do not exhibit such behavior. Thus, the lower-limited of ς is 0.5[18]. Based on the measured values of residual stress, coefficients of the exponentially damped cosine function

https://doi.org/10.1017/aer.2018.151 Published online by Cambridge University Press

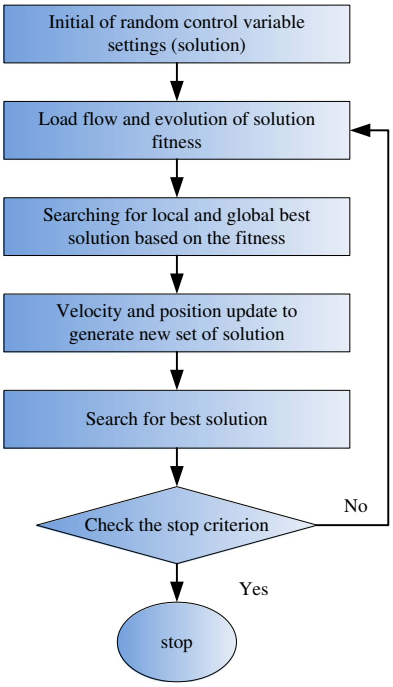

Figure 8. (Colour online) The flow chart of PSO method.

in both σ_1 and σ_3 directions are optimised, and the results are shown in Tables 3 and 4, respectively.

In Tables 3 and 4, R^2 is the linear correlation coefficient, and the value of R^2 lies in the range [0, 1], with '1' indicating a perfect fit and '0' indicating an imperfect one. It can be deduced from the results of R^2 that the proposed function gives a high precision to represent the machining-induced residual stress profile.

In Equation (7), Young's modulus (E) of Ti–6Al–4V is 110×10^9 Pa, and the width of cut (d) is 5 mm.

With the data of Young's modulus, feed speed, width of cut and the exponentially damped cosine functions of σ_1 and σ_3, machining-induced surface energy P_{cut}, which unit in SI (kg/m/s) unit system is watt, was calculated. The values of the surface energy were in the range of 0.16–33.65 W, and the maximum value was get under the cutting condition of G16, while the minimum value for G03. The influence of cutting parameters on the value of machining-induced surface energy was analysed, as shown in Fig. 9.

According to Fig. 9, with the increase of cutting speed, the machining-induced surface energy tends to become larger. This is probably due to the large cutting force under the condition of high cutting speed. It also can be found that the machining-induced surface energy gets larger with the increase of feed rate, which can be proved by Equation (7) that the strain energy stored in unit time during the machining process is directly proportional to the feed speed. In addition, the strain energy stored in unit time has little change with the varied a_e for the fact of that it has little effect on the four key factors of residual stress profile. Different from linear relation of surface energy to cutting speed v_c and feed rate f_z, the effect of depth of cut a_e on surface energy is weakened when the value of a_e is greater than 1.5 mm. Furthermore, analysis of variance showed that the feed rate was the main factor affecting the

https://doi.org/10.1017/aer.2018.151 Published online by Cambridge University Press

Table 3
Results of the optimised coefficients in σ_1 direction (partial)

No.	C_0 (MPa)	w_d (μm^{-1})	φ (rad)	ς (–)	R^2 (%)
G03	1,285.27	88.46	1.87	0.859	99.50
G04	1,653.55	92.85	1.43	0.810	87.61
G07	5,052.66	29.29	1.62	0.981	95.85
G08	5,783.18	20.52	1.51	0.990	70.20
G11	1,804.25	140.23	1.84	0.704	92.00
G12	3,064.62	78.16	1.57	0.908	92.19
G15	1,984.64	148.15	1.77	0.754	97.29
G16	6,884.45	28.52	1.56	0.986	92.46

Table 4
Results of the optimised coefficients in σ_3 direction (partial)

No.	C_0 (MPa)	w_d (μm^{-1})	φ (rad)	ς (–)	R^2 (%)
G03	432.08	134.38	2.10	0.554	97.70
G04	558.62	122.44	1.90	0.696	99.10
G07	968.13	108.17	1.68	0.685	97.69
G08	1,398.25	66.54	1.57	0.818	96.00
G11	2,322.19	37.13	1.54	0.896	96.05
G12	3,692.40	26.76	1.55	0.959	96.89
G15	1,771.48	42.03	1.46	0.815	98.00
G16	1,419.06	40.81	1.45	0.734	96.88

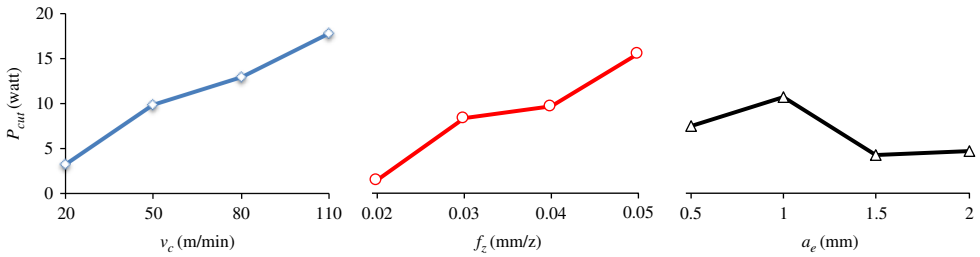

Figure 9. (Colour online) Relationship of surface energy with cutting parameters.

machining-induced surface energy, followed by the depth of cut and cutting speed, respectively.

4.3 Effects of residual stress and surface energy on fatigue life

The fatigue test results show that the life range of the sample for case one is 2,510–8,141 cycles, and the life range for case two is 16,709–3,5341 cycles, which are shown in Fig. 10.

https://doi.org/10.1017/aer.2018.151 Published online by Cambridge University Press

Accordingly, the maximum fatigue life is increased by 434.1% with the maximum fatigue stress reduced 200 MPa.

The changes of fatigue life against the four key factors of the residual stress profile are shown in Figs. 11–14. As shown in Fig. 11, surface residual compressive stress is beneficial to prolong the fatigue life, and fatigue life is obviously improved with the increase of the surface residual compressive stress for both cases of one and two. It is mainly because most of the fatigue fracture of structural parts made from industrial alloys originates from the surface of the material[19], surface residual compressive stress makes the nucleation and propagation of fatigue cracks more difficult. In addition, according to Westergaard's[20] analysis of the

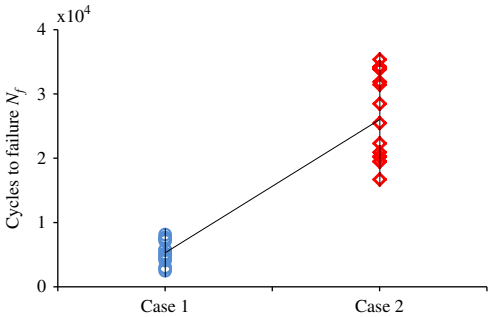

Figure 10. (Colour online) Fatigue life under various loading conditions.

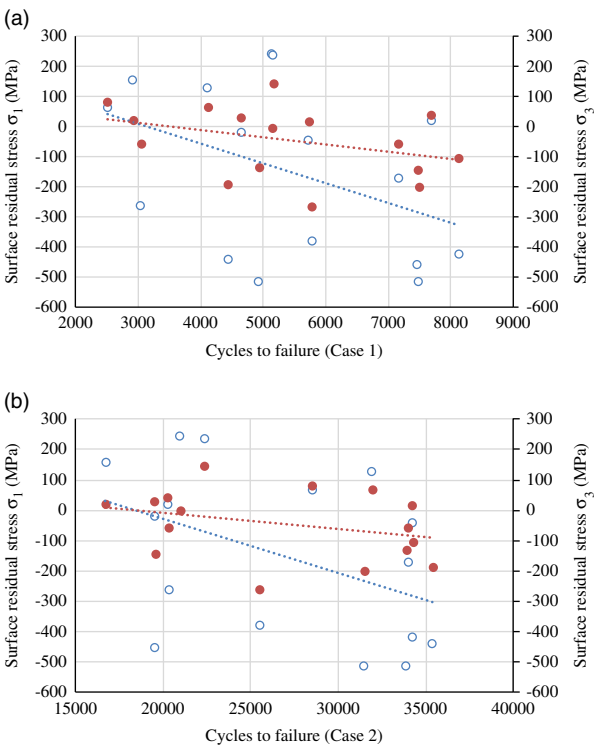

Figure 11. (Colour online) Effect of the surface residual stress on fatigue life.

https://doi.org/10.1017/aer.2018.151 Published online by Cambridge University Press

stress field at the tip of fatigue crack, stress intensity factor K dominants the distribution of the stress field at the crack tip, and it will be the equivalent stress intensity factor K_{eff}, which is coupled with the residual stress intensity factor and the initial stress intensity factor when the alternating load is acted separately. Therefore, the fatigue crack growth rate increases and the service life of part reduced. Meanwhile, compressive residual stress plays the opposite role.

For the reason that the direction of σ_3 is perpendicular to the direction of tensile–tensile load, surface residual compressive stress in σ_3 direction has a weak impact on fatigue life. Therefore, the influence of residual stress in σ_3 direction will not be considered later. According to Figs 12 and 13, results show that the maximum compressive residual stress leads to an increase of fatigue life, while the effect decreases with the location of the maximum residual stress far away from the machined surface. Fig. 14 shows that the large depth of residual stress is not conducive to prolong the fatigue life.

As discussed above, it is hard to find the best combination of the four factors of the residual stress profile to get the best fatigue performance of the machined titanium alloy Ti–6Al–4V. Fatigue is an irreversible process of energy dissipation. In the process of fatigue, a part of the external machinery energy can be absorbed by the material, and the absorbed energy has a direct relationship with the fatigue life of the specimen[21]. According to Feltner[22], there is an energy threshold W_f for material fracture, which has nothing to do with loading history. The fatigue damage energy is the accumulation of plastic strain energy of materials under cyclic loading[23,24], and the existence of initial plastic strain energy (machining-induced

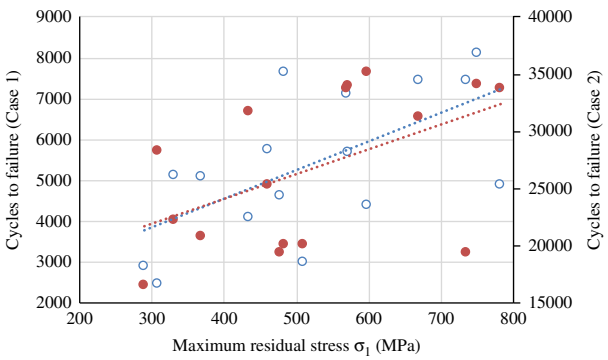

Figure 12. (Colour online) Effect of the maximum residual stress on fatigue life.

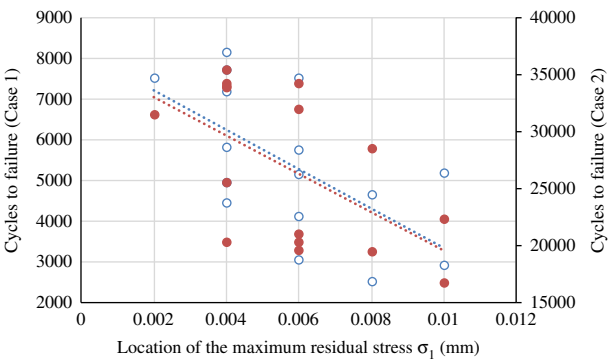

Figure 13. (Colour online) Effect of location of the maximum residual stress on fatigue life.

https://doi.org/10.1017/aer.2018.151 Published online by Cambridge University Press

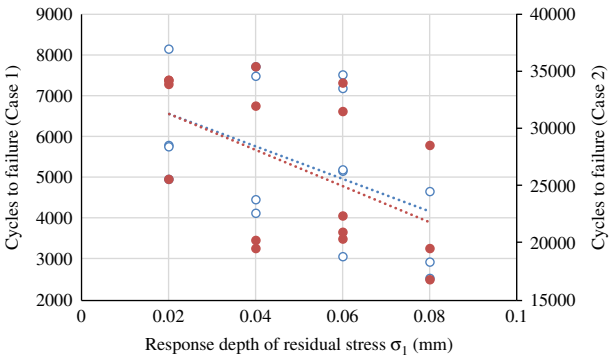

Figure 14. (Colour online) Effect of the response depth of residual stress on fatigue life.

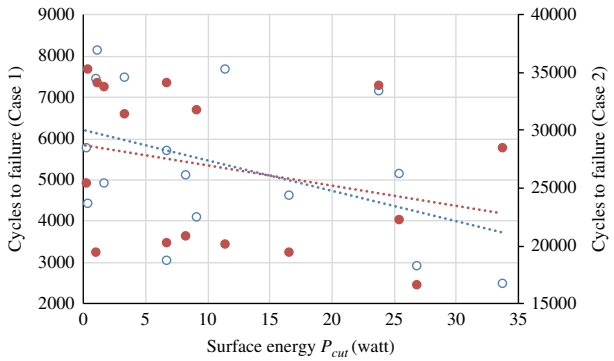

Figure 15. (Colour online) Effect of machining-induced surface energy on fatigue life.

Table 5
ANOVA tests results

Source of variance	Case number	$\sigma_{r,Sur}$	$\sigma_{C,ax}$	h_{r0}	h_{ry}	P_{cut}
F ratio	Case 1	150.4145	174.0618	145.9831	145.9831	145.9805
	Case 2	253.9423	261.3274	251.5981	251.5972	251.3918
P value	Case 1	3.23E – 13	5.04E – 14	4.7E – 13	4.7E – 13	4.7E – 13
	Case 2	3.47E – 16	2.36E – 16	3.94E – 16	3.94E – 16	3.98E – 16

surface energy) will inevitably lead to the increase of fatigue damage energy, which accelerates fatigue failure. Therefore, large values of machining-induced surface energy lead to a decrease of fatigue life, which is shown in Fig. 15.

To determine the significance of the factors of the residual stress on fatigue performance, the analysis of variance (ANOVA) tests was conducted. In the present study, a significance level of 0.05 (confidence level of 95%) was selected, and ANOVA results for the factors of residual stress are presented in Table 5. According to ANOVA analyses, values of statistic level *P* are much less than 0.05, which means that all the factors of residual stress have

https://doi.org/10.1017/aer.2018.151 Published online by Cambridge University Press

significant effects on fatigue performance of the machined titanium alloy Ti–6Al–4V. The values of the significant difference level F ratio indicate that the effect of $\sigma_{C,ax}$ on fatigue life is larger than other factors of residual stress for both cases 1 and 2. In addition, fatigue performance of case 2 is more sensitive to the machining-induced residual stress than that of case 1, which means that the effect of residual stress on fatigue life decreased with the increase of fatigue load.

5.0 CONCLUSION

In the present study, residual stress profile induced by peripheral milling of Ti–6Al–4V was first studied. And then, energy criteria for machining-induced residual stress field, named surface energy, were proposed to characterise the whole stated of the residual stress field. Finally, the effect of machining-induced residual stress and its energy property on fatigue performance of titanium alloy Ti–6Al–4V were discussed. The following conclusions were derived according to the researches:

Variation trend of surface residual stress ($\sigma_{r,Sur}$), maximum compressive residual stress ($\sigma_{C,ax}$), location (h_{r0}) and response depth (h_{ry}) with cutting parameters showed a similar pattern for both measure directions those parallel (σ_1) and perpendicular (σ_3) to the cutting direction in the machined surface. Cutting speed and feed rate have a main effect on surface residual stress, and the depth of cut has little effect on all four key factors of residual stress profile.

With the increase of cutting speed and feed rate, machining-induced surface energy tended to become larger. But increasing the depth of cut caused the strain energy stored in unit time to decrease. Furthermore, the effect of depth of cut on surface energy was weakened when the value of cutting depth was greater than 1.5 mm.

Both the surface compressive residual stress and the maximum compressive residual stress are good for prolonging the fatigue life. While the large value of machining-induced surface energy led to a decrease of fatigue life, it was for the fact of the fatigue life is in inverse proportion to the values of the location of maximum compressive stress and response depth of residual stress. According to ANOVA analysis, maximum compressive stress has a greater impact on fatigue life than other residual stress factors.

ACKNOWLEDGEMENTS

This work was supported by the Key Natural Science Project of Anhui Provincial Education Department (KJ2018A0021) and High-level talent fund of Anhui University.

REFERENCES

1. XIONG, R. and WU, H. Study on cutting mechanism of Ti6Al4V in ultra-precision machining, *Int J Advanced Manufacturing Technology*, 2016, **86**, (5–8), pp 1–7.
2. ZHANG, G., LIU, J., LIU, Y. and YUE, Z. Effect of roughness on surface stress concentration factor and fatigue life, *J Mech Strength*, 2010, **32**, (1), pp 023.
3. JAVIDI, A., RIEGER, U. and EICHLSEDER, W. The effect of machining on the surface integrity and fatigue life, *Int J of fatigue*, 2008, **30**, (10–11), pp 2050–2055.
4. SHARMAN, A.R.C., ASPINWALL, D.K., DEWES, R.C., CLIFTON, D. and BOWEN, P. The effects of machined workpiece surface integrity on the fatigue life of γ-titanium aluminide, *Int J Machine Tools and Manufacture*, 2001, **41**, (11), pp 1681–1685.

https://doi.org/10.1017/aer.2018.151 Published online by Cambridge University Press

5. LIU, G.L., HUANG, C.Z., ZOU, B. and LIU, Z.Q. Surface integrity and fatigue performance of 17-4PH stainless steel after cutting operations, *Surface and Coatings Technology*, 2016, **307**, pp 182–189.
6. LI, Y.J., XUAN, F.Z., WANG, Z.D. and TU, S.T. Effects of residual stresses on the high cycle fatigue behavior of Ti–6Al–4V, ASME 2010 Pressure Vessels and Piping Division/K-PVP Conference, *American Society of Mechanical Engineers*, 2010, pp 397–401.
7. SMITH, S., MELKOTE, S.N., LARA-CURZIO, E., WATKINS, T.R., ALLARD, L. and RIESTER, L. Effect of surface integrity of hard turned AISI 52100 steel on fatigue performance, *Materials Science and Engineering: A*, 2007, **459**, (1–2), pp 337–346.
8. FARRAHI, G.H., LEBRIJN, J.L. and COURATIN, D. Effect of shot peening on residual stress and fatigue life of a spring steel, *Fatigue and Fracture of Engineering Materials and Structures*, 1995, **18**, (2), pp 211–220.
9. GUO, Y.B. and YEN, D.W. Hard turning versus grinding – the effect of process-induced residual stress on rolling contact, *Wear*, 2004, **256**, (3–4), pp 393–399.
10. GUO, Y.B. and BARKEY, M.E. Modeling of rolling contact fatigue for hard machined components with process-induced residual stress, *Int J of fatigue*, 2004, **26**, (6), pp 605–613.
11. SUN, J. and GUO, Y.B. A comprehensive experimental study on surface integrity by end milling Ti–6Al–4V, *J Materials Processing Technology*, 2009, **209**, (8), pp 4036–4042.
12. SRIDHAR, B.R., DEVANANDA, G., RAMACHANDRA, K. and BHAT, R. Effect of machining parameters and heat treatment on the residual stress distribution in titanium alloy IMI-834, *J Materials Processing Technology*, 2003, **139**, (1–3), pp 628–634.
13. GUERVILLE, L., VIGNEAU, J., DUDZINSKI, D., MOLINARI, A. and SCHULZ, H. Influence of machining conditions on residual stresses, Metal Cutting and High-Speed Machining, Kluwer Academic Plenum Publishers, New York, US, 2002, pp 201–210.
14. MANTLE, A.L. and ASPINWALL, D.K. Surface integrity of a high speed milled gamma titanium aluminide, *J Materials Processing Technology*, 2001, **118**, (1–3), pp 143–150.
15. YANG, D., LIU, Z.Q., REN, X.P. and ZHUANG, P. Hybrid modeling with finite element and statistical methods for residual stress prediction in peripheral milling of titanium alloy Ti–6Al–4V, *Int J of Mechanical Sciences*, 2016, **108**, pp 29–38.
16. VOSOUGH, M., KALHORI, V., LIU, P. and SVENNINGSSON, I. Influence of High Pressure Water-Jet Assisted Turning on Surface Residual Stresses on Ti–6Al–4V Alloy by Measurement and Finite Element Simulation, In Surface Engineering, *Proceedings of the 3rd International Surface Engineering Congress*, 2005, pp 107–113.
17. ULUTAN, D. Predictive Modeling and Multi-objective Optimization of Machining-Induced Residual Stresses: Investigation of Machining Parameter Effects, Dissertations & Theses, Gradworks, 2013.
18. ULUTAN, D., ARISOY, Y.M., ÖZEL, T. and MEARS, L. Empirical modeling of residual stress profile in machining nickel-based super alloys using the sinusoidal decay function, *Procedia CIRP*, 2014, **13**, pp 365–370.
19. SRIKANTH, R., KOSMAC, T., BONA, A.D., YIN, L. and ZHANG, Y. Effects of cementation surface modifications on fracture resistance of zirconia, *Dental Materials*, 2015, **31**, (4), pp 435–442.
20. WESTERGAARD, H.M. Bearing pressures and cracks, *Spie Milestone Series Ms*, 1997, **137**, pp 18–22.
21. WANG, X.G., CRUPI, V., GUO, X.L. and ZHAO, Y.G. Quantitative thermographic methodology for fatigue assessment and stress measurement, *Int J of fatigue*, 2010, **32**, (12), pp 1970–1976.
22. FELTNER, C.E. and MORROW, J.D. Microplastic strain hysteresis energy as a criterion for fatigue fracture, *J of Basic Engineering*, 1961, **83**, (1), pp 15–22.
23. MORROW, J.D. Cyclic Plastic Strain Energy and Fatigue of Metals. Internal Friction, Damping, and Cyclic Plasticity, *ASTM Int*, 1965.
24. MACEK, W., ŁAGODA, T. and MUCHA, N. Energy-based fatigue failure characteristics of materials under random bending loading in elastic-plastic range, *Fatigue & Fracture of Engineering Materials & Structures*, 2018, **41**, (2), pp 249–259.

https://doi.org/10.1017/aer.2018.151 Published online by Cambridge University Press